


# Optical temporal interference model for investigation and manipulation of non-integer high-order harmonic generation

Zhao-Yue Meng(孟昭越), Yun Pan(潘云), Jun-Ping Wang(王军平), and Xi Zhao(赵曦)
**Citation:**Chin. Phys. B, 2026, 35 (**2**): 024208. DOI: 10.1088/1674-1056/adfdc5
http://cpb.iphy.ac.cn; http://iopscience.iop.org/cpb

**What follows is a list of articles you may be interested in**

---

## 3D-GTDSE: A GPU-based code for solving 3D-TDSE in Cartesian coordinates

Ke Peng(彭科), Aihua Liu(刘爱华), Jun Wang(王俊), and Xi Zhao(赵曦)
Chin. Phys. B, 2025, 34 (**9**): 094203. DOI: 10.1088/1674-1056/adee00

## Elliptically polarized high-order harmonic generation of Ar atom in an intense laser field

Jie Hu(胡杰), Yi-Chen Wang(王一琛), Qiu-Shuang Jing(景秋霜), Wei Jiang(姜威), Ge-Wen Wang(王革文), Yi-Wen Zhao(赵逸文), Bo Xiao(肖礴), Hong-Jing Liang(梁红静), and Ri Ma(马日)
Chin. Phys. B, 2024, 33 (**5**): 054208. DOI: 10.1088/1674-1056/ad2604

## Tunable spectral continuous shift of high-order harmonic generation in atoms by a plasmon-assisted shaping pulse

Yuan Wang(王源), Yulong Li(李玉龙), Yue Qiao(乔月), Na Gao(高娜),Fu-Ming Guo(郭福明), Zhou Chen(陈洲), Lan-Hai He(赫兰海),Yu-Jun Yang(杨玉军), Xi Zhao(赵曦), and Jun Wang(王俊)
Chin. Phys. B, 2024, 33 (**3**): 034212. DOI: 10.1088/1674-1056/ad10fb

## Calibration of quantitative rescattering model for simulating vortex high-order harmonic generation driven by Laguerre-Gaussian beam with nonzero orbital angular momentum

Jiaxin Han(韩嘉鑫), Zhong Guan(管仲), Beiyu Wang(汪倍羽), and Cheng Jin(金成)
Chin. Phys. B, 2023, 32 (**12**): 124210. DOI: 10.1088/1674-1056/acfa86

## Spectral shift of solid high-order harmonics from different channels in a combined laser field

Dong-Dong Cao(曹冬冬), Xue-Fei Pan(潘雪飞), Jun Zhang(张军), and Xue-Shen Liu(刘学深)
Chin. Phys. B, 2023, 32 (**3**): 034204. DOI: 10.1088/1674-1056/aca4bf

---

# Optical temporal interference model for investigation and manipulation of non-integer high-order harmonic generation

Zhao-Yue Meng(孟昭越)[1,2,3], Yun Pan(潘云)[4], Jun-Ping Wang(王军平)[1,†], and Xi Zhao(赵曦)[2]

[1] *School of Physics, Liaoning University, Shenyang* 110036, *China*
[2] *School of Physics and Information Technology, Shaanxi Normal University, Xi'an* 710062, *China*
[3] *School of Materials and New Energy, South China Normal University, Shanwei* 516625, *China*
[4] *School of Science, Shenyang Institute of Engineering, Shenyang* 110136, *China*

(Received 29 May 2025; revised manuscript received 26 July 2025; accepted manuscript online 21 August 2025)

High-precision optical frequency measurement serves as a cornerstone of modern science and technology, enabling advancements in fields ranging from fundamental physics to quantum information technologies. Obtaining precise photon frequencies, especially in the ultraviolet or even extreme ultraviolet regimes, is a key goal in both light–matter interaction experiments and engineering applications. High-order harmonic generation (HHG) is an ideal light source for producing such photons. In this work, we propose an optical temporal interference model (OTIM) that establishes an analogy with multi-slit Fraunhofer diffraction (MSFD) to manipulate fine-frequency photon generation by exploiting the temporal coherence of HHG processes. Our model provides a unified physical framework for three distinct non-integer HHG generation schemes: single-pulse, shaped-pulse, and laser pulse train approaches, which correspond to single-MSFD-like, double-MSFD-like, and multi-MSFD-like processes, respectively. Arbitrary non-integer HHG photons can be obtained using our scheme. Our approach provides a new perspective for accurately measuring and controlling photon frequencies in fields such as frequency comb technology, interferometry, and atomic clocks.

**Keywords:** high-order harmonic generation, optical temporal interference, multi-slit Fraunhofer diffraction

**PACS:** 42.65.Ky, 42.65.Re

**DOI:** 10.1088/1674-1056/adfdc5 **CSTR:** 32038.14.CPB.adfdc5

## 1. Introduction

The highly accurate measurement of optical frequency has transformed precision metrology and its applications across a wide range of fields. From the calibration of atomic clocks to high-resolution spectroscopy and telecommunications, the ability to measure frequencies with extreme precision has led to significant technological advancements and a deeper understanding of fundamental physical principles.[1–6] As the technology continues to evolve, it is expected to unlock new possibilities and drive further innovation in science and industry.[7–10]

So far, the synergy between high-order harmonic generation (HHG) and highly accurate optical-frequency measurement has driven advancements in both fields and attracted considerable attention.[11–26] HHG is a non-linear optical process in which intense laser fields interact with a medium, typically a gas or a crystal, to generate radiation at integer multiples of the laser frequency. This process produces coherent light spanning the extreme ultraviolet to soft x-ray regions while simultaneously enabling the generation of attosecond pulses.[27–37] Explained by the three-step model (ionization, acceleration, and recombination of electrons), this phenomenon has enabled applications in attosecond science, including studies of real-time electron dynamics, high-resolution spectroscopy, and imaging in material science and biomedical fields. Despite challenges in efficiency, phase matching, and scalability, HHG shows great potential for high-precision metrology and the development of robust industrial applications, driven by ongoing research efforts to enhance its capabilities.[38–46]

Understanding and generating non-integer HHG (also referred to as HHG sidebands) represents a crucial advancement in highly accurate optical-frequency measurement and attosecond science, offering significant benefits across diverse scientific and technological domains.[47–53] This capability extends spectral coverage and provides tunable photon energies, which are essential for high-resolution spectroscopy and element-specific probing. In imaging, non-integer HHG enhances contrast and resolution, improving techniques such as phase-contrast imaging. These photons also play a pivotal role in advanced non-linear optics, facilitating wave mixing and frequency comb generation, thereby expanding opportunities in precision metrology and clock synchronization. Fundamental research in attosecond science and quantum dynamics further benefits from improved temporal resolution and enhanced control over quantum states.[54,55]

The generation of non-integer HHG typically requires modification of either the driving laser field characteristics or the interaction conditions to disrupt the strict periodicity of

†Corresponding author. E-mail: wangjp@lnu.edu.cn

© 2026 Chinese Physical Society and IOP Publishing Ltd. All rights, including for text and data mining, AI training, and similar technologies, are reserved.

the field. This can be achieved through several approaches, including spectral amplitude or phase modulation of the driving laser pulse, or the use of a frequency comb laser source.[56–61] The latter approach employs a series of equally spaced frequency components to produce a spectrum containing non-integer HHG.

In this work, we employ the optical temporal interference model (OTIM) to systematically investigate the physical mechanisms underlying non-integer HHG through precise temporal control of laser pulse structures. We examine three distinct generation schemes: (i) a single trapezoidal-envelope pulse scheme, which provides a conceptually clear demonstration of the OTIM framework due to its simple temporal structure, despite being experimentally challenging to implement; (ii) a $\pi$-phase-modulated shaped-pulse approach that enables precise spectral control; and (iii) an optical frequency comb scheme based on laser pulse sequences, capable of generating well-defined frequency comb structures in the HHG spectrum.

## 2. Theoretical model

The OTIM fundamentally relies on the temporal coherence of HHG photon emission processes. Our model demonstrates that precise control over both the temporal intervals and the multiplicity of HHG photons enables direct manipulation of this quantum-coherent process. Remarkably, the underlying physical mechanism exhibits a profound analogy to optical multi-slit Fraunhofer diffraction (MSFD). Within the OTIM framework, we establish that all three temporal control schemes for non-integer HHG generation share an identical fundamental physical origin. Moreover, this model provides a systematic approach for precise spectral control of non-integer HHG.

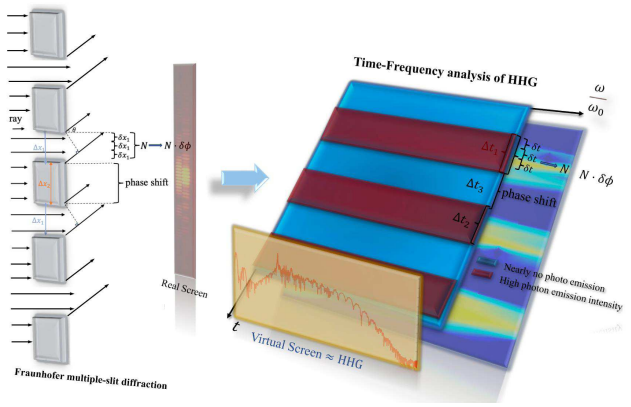



**Fig. 1.** The left panel illustrates Fraunhofer multi-slit diffraction, whereas the right panel displays the time–frequency analysis of HHG. Here, $N$ represents the number of slits, and $\theta$ denotes the diffraction angle. $\Delta x_1$ and $\Delta x_2$ denote the slit width and the spacing between adjacent slits, respectively. $\Delta t_1$ and $\Delta t_2$ represent two emission-burst time windows, while $\Delta t_3$ denotes the temporal delay between these emission bursts. A coherent summation of photons along the time axis ($t$-axis) in the time–frequency domain renders this process analogous to Fraunhofer multiple-slit diffraction.

As illustrated in Fig. 1 (left panel), the system can be modeled as an $N$-slit diffraction apparatus. The total optical wave passing through the slits at an emission angle $\theta$ yields an amplitude given by

$$A = A_0 \left(\frac{\sin\alpha}{\alpha}\right)\left(\frac{\sin N\beta}{\sin\beta}\right), \tag{1}$$

where $A_0$ is the resultant amplitude. The phase terms in our diffraction model are defined as $\alpha = \Delta\phi_1/2$ and $\beta = \Delta\phi_2/2$, with the fundamental phase differences given by $\Delta\phi_1 = (\lambda/2\pi)\Delta x_1 \sin\theta$ and $\Delta\phi_2 = (\lambda/2\pi)\Delta x_2 \sin\theta$. Here, $\Delta x_1$ and $\Delta x_2$ denote the slit width and the spacing between adjacent slits, respectively. Thus, $\Delta\phi_1$ represents the phase difference between the top and bottom of the slit at the angle $\theta$.

The right panel of Fig. 1 displays the calculated time–frequency analysis spectrum of the high-harmonic generation process, obtained through a Gabor transform of the time-dependent dipole acceleration.[62] The red features correspond to distinct attosecond photon emission bursts occurring within two characteristic time intervals, $\Delta t_1$ and $\Delta t_2$, which are separated by a well-defined temporal delay $\Delta t_3$.

Following Eq. (1), we express the total HHG amplitude $H(\omega)$ at photon energy $\omega$ as the coherent superposition of $N$ discrete emission events

$$H(\omega) = H_0 \left(\frac{\sin\left(\frac{\omega\Delta t_1}{2}\right)}{\frac{\omega\Delta t_1}{2}}\right)\left(\frac{\sin\left(N\frac{\omega\Delta t_3}{2}\right)}{\sin\left(\frac{\omega\Delta t_3}{2}\right)}\right). \tag{2}$$

The interference term $\sin\left(N\frac{\omega\Delta t_3}{2}\right)/\sin\left(\frac{\omega\Delta t_3}{2}\right)$ represents the characteristic multi-slit diffraction factor, which gives rise to a diffraction pattern in the HHG spectrum characterized by principal maxima and secondary maxima. The total number of secondary maxima $G$ is directly determined by the number of temporal slits $N$ (i.e., discrete HHG photon emission events), following the relation:[63]

$$G = N - 2. \tag{3}$$

Our simulations are based on the widely used strong-field approximation (SFA) model for HHG (detailed mathematical expressions for SFA-based HHG can be found in Ref. [64]). Atomic units are used throughout this work, unless otherwise mentioned.

## 3. Results and discussion

### 3.1. Single trapezoidal envelope pulse case

We first validate the OTIM framework by simulating HHG driven by a single trapezoidal pulse. As noted earlier, this trapezoidal profile is primarily a mathematical construct, offering a straightforward case for demonstrating OTIM. In Fig. 2(b), we present the HHG spectra generated by a trapezoidal envelope pulse (red line in Fig. 2(a)) and a Gaussian envelope pulse (blue dotted line in Fig. 2(a)) interacting with a

He atom. The two pulses share similar laser parameters: both have amplitudes of 0.092 (corresponding to $3\times10^{14}$ W/cm$^2$) and wavelengths of 800 nm (corresponding to a laser frequency of $\omega_0 = 0.057$). The Gaussian envelope pulse has a full width at half maximum (FWHM) duration of 8 optical cycles (o.c.), while the trapezoidal pulse consists of a 1-cycle linear ramp-up, a 5-cycle plateau, and a 1-cycle linear ramp-down.

For HHG driven by a trapezoidal pulse, we observe seven sidebands between adjacent odd-order peaks in the high-energy region near the spectral cutoff. In contrast, such sidebands do not appear in the HHG spectrum produced by a Gaussian pulse. This difference originates from the distinct envelope structures: the trapezoidal electric field maintains a highly regular periodic structure with stable peak intensities, whereas the Gaussian envelope lacks this degree of temporal uniformity. Therefore, we can approximate $\Delta t_1 = \Delta t_3 = \pi/\omega_0$ in Eq. (2), leading to the HHG amplitude at photon energy $\omega$ driven by a trapezoidal pulse

$$H(\omega) = H_0 \frac{\sin\left(\frac{N\pi}{2}\cdot M\right)}{\left(\frac{\omega\Delta t_3}{2}\right)} \quad , \quad N, M \in \mathbb{Z}^+. \tag{4}$$

Here, $M = \omega/\omega_0$ represents the harmonic order. Furthermore, when $M$ is even, $N\cdot M/2$ always yields an integer, leading to $H = 0$. Consequently, even-order harmonics vanish. In contrast, when the harmonic order is odd, constructive interference occurs, explaining the exclusive presence of odd-order harmonic peaks in the HHG spectrum.

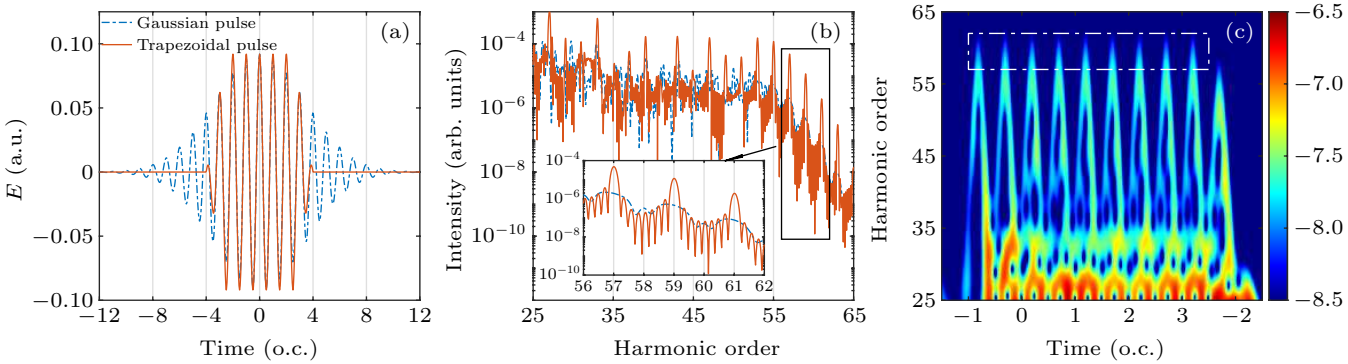



**Fig. 2.** (a) The red solid line and blue dashed line correspond to trapezoidal and Gaussian envelope laser pulses, respectively, both with a peak intensity of 0.092 a.u. and a central wavelength of 800 nm. The Gaussian pulse has a FWHM duration of 8 optical cycles (o.c.), whereas the trapezoidal pulse features a 1-cycle linear ramp-up, a 5-cycle constant-intensity plateau, and a 1-cycle linear ramp-down. (b) The red solid line and blue dashed line show the HHG spectra produced by the two laser fields shown in panel (a). A zoomed-in view between the 56th and 62nd harmonic orders reveals sidebands between adjacent odd-order peaks in the HHG spectrum generated by the trapezoidal pulse. (c) Time–frequency analysis of HHG produced by the trapezoidal laser field. The white box indicates the emission time corresponding to the zoomed-in harmonic spectrum shown in panel (b).

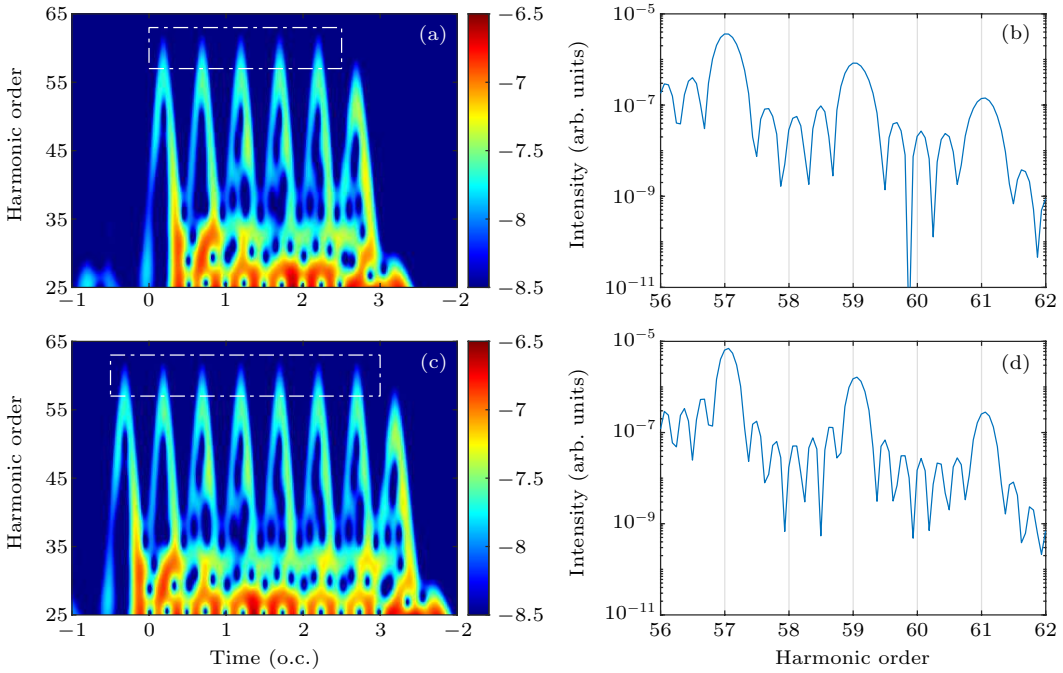



**Fig. 3.** (a) Time–frequency analysis of HHG generated by a trapezoidal laser field with a 3-cycle constant-intensity plateau. (b) Corresponding HHG spectra in the 56th–62nd harmonic-order range (white box region in panel (a)). (c) Time–frequency analysis of HHG generated by a trapezoidal laser field with a 4-cycle constant-intensity plateau. (d) Corresponding HHG spectra in the 56th–62nd harmonic-order range (white box region in panel (c)).

As shown in Fig. 2(c), the time–frequency analysis of the HHG spectra generated by the trapezoidal laser field [Fig. 2(a)] reveals nine temporal slits, as indicated by the white box. According to Eq. (3), this configuration should produce seven sidebands between consecutive odd-order harmonic peaks. Consistent with this theoretical prediction, these sidebands are clearly observed in Fig. 2(b).

Similar features are observed in Fig. 3. Figure 3(a) displays the time–frequency analysis for a trapezoidal pulse featuring a 3-cycle plateau region, where five temporal slits appear near the cutoff region, as marked by the white box. Consistent with this observation, three well-resolved sidebands emerge in the corresponding HHG spectrum. Figure 3(c) presents analogous results for a 4-cycle plateau pulse, showing seven temporal slits near the cutoff region and five associated sidebands. These results further demonstrate the universality of the OTIM model.

### 3.2. Shaped-pulse case

Non-integer HHG from trapezoidal laser pulses can be analyzed using a single-MSFD-like model. Next, we extend this approach to a double-MSFD-like model. The red curve in Fig. 4(a) represents a $\pi$-phase-shaped pulse generated by manipulating an input Gaussian envelope pulse (blue curve in Fig. 4(a)). The input Gaussian envelope pulse has a central wavelength of 800 nm, a peak field strength of 0.092 a.u., and a full width at half maximum (FWHM) of 2 o.c. Experimentally, such $\pi$-phase-shaped pulses can be generated using a liquid crystal spatial light modulator (SLM).[65,66] Mathematically, the shaped pulse in the frequency domain, $\tilde{E}_{\rm out}(\omega)$, is obtained by applying a spectral phase modulation to the input Gaussian pulse, $\tilde{E}_{\rm out}(\omega)=\tilde{E}_{\rm in}(\omega)\,{\rm e}^{{\rm i}\phi(\omega)}$, where the phase function $\phi(\omega)$ is defined as the following piecewise function

$$\phi(\omega)=\begin{cases}0, & \omega<\omega_0,\\ \pi, & \omega\geq\omega_0.\end{cases} \tag{5}$$

Here, $\omega_0$ represents the central frequency of the input pulse. The $\pi$-phase-shaped pulse in the time domain, $E_{\rm out}(t)$, is then obtained through an inverse Fourier transform of the frequency-domain field: $E_{\rm out}(t)={\rm IFFT}(\tilde{E}_{\rm out})$.

Figure 4(a) shows that the time-domain shaped pulse $E_{\rm out}(t)$ exhibits a characteristic double-peak structure, with peaks centered at $t=\pm1.21$ o.c. The corresponding HHG spectrum, shown in Fig. 4(b), displays pronounced sideband features near the cutoff region. In the following analysis, we employ our theoretical model to quantitatively explain the origin of these HHG sideband structures.

In this scenario, each peak of the shaped pulse $E_{\rm out}(t)$ acts as a temporal slit, with the two slits separated by a time interval $\Delta t_4$, analogous to the opaque spacing in an optical double-MSFD experiment. Consequently, the HHG signals from these two temporal slits interfere, yielding the total HHG signal

$$H(\omega)=H_{d-0}+H_{d-1}\,{\rm e}^{{\rm i}\omega\Delta t_4}, \tag{6}$$

where $H_{d-0}$ and $H_{d-1}$ represent the HHG signals from the first and second temporal slits, respectively. Given the identical nature of the two laser peaks, we can approximate $H_{d-0}=H_{d-1}=b$. The resulting total HHG signal intensity is therefore

$$|H(\omega)|^2=2b^2\left[1+\cos\left(\omega\Delta t_4\right)\right]. \tag{7}$$

From Eq. (7), it is straightforward to observe that the HHG signal exhibits a peak–valley structure, with peak positions $\omega_d$ given by $\omega_d=\frac{2k\pi}{\Delta t_4}$, where $k\in\mathbb{Z}$. Consequently, the sideband spacing ($\Delta E_d$) in the double-MSFD-like scenario is $\Delta E_d=\frac{2\pi}{\Delta t_4}$. If we express $\Delta E_d$ in units of $\omega_0$ (analogous to HHG orders), the non-integer HHG order becomes

$$\Delta N=\frac{\Delta E_d}{\omega_0}=\frac{1}{\Delta T}, \tag{8}$$

where $\Delta T$ is $\Delta t_4$ normalized by the optical cycle.

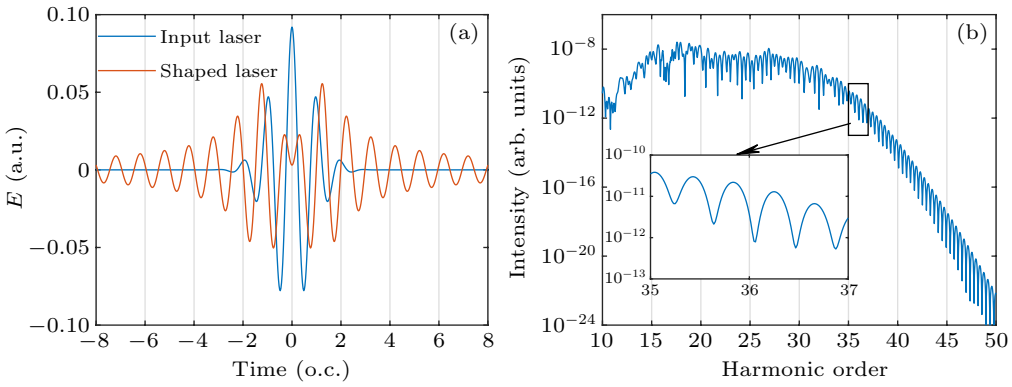



**Fig. 4.** (a) Temporal profile of a $\pi$-phase-shaped laser pulse (red solid line), exhibiting a characteristic double-peak structure. The pulse is generated from an input pulse (blue solid line) with a central wavelength of 800 nm, a peak field strength of 0.092 a.u., and a FWHM of 2 o.c. (b) HHG spectrum produced by the shaped pulse shown in panel (a), revealing distinct and equidistant peaks in the high-energy region, confirming the formation of a harmonic frequency comb.

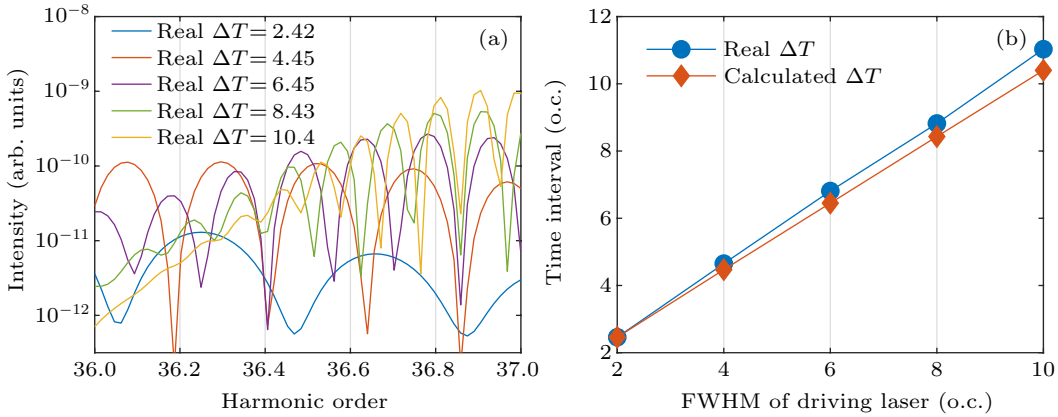



**Fig. 5.** (a) HHG spectra generated by $\pi$-phase-shaped pulses with different real $\Delta T$ values. As the real $\Delta T$ increases, the spectra exhibit a clear reduction in the optical frequency comb spacing ($\Delta N$), although the rate of this decrease gradually slows. (b) Comparison between the real $\Delta T$ and the theoretically calculated $\Delta T$. The excellent agreement validates the accuracy of our theoretical model.

To verify this relationship, we systematically adjusted the FWHM of the input Gaussian pulse to 2 o.c., 4 o.c., 6 o.c., 8 o.c., and 10 o.c., which generated $\pi$-phase-shaped laser pulses with corresponding real $\Delta T$ values of 2.42 o.c., 4.45 o.c., 6.45 o.c., 8.43 o.c., and 10.4 o.c., respectively. Figure 5(a) presents the resulting HHG spectra of these shaped pulses. As predicted by our model, the observed $\Delta N$ decreases with increasing $\Delta T$, confirming the inverse relationship between these two parameters.

To further validate our model, Fig. 5(b) compares the real $\Delta T$ values with those calculated using our model (Eq. (8)) based on the $\Delta N$ extracted from the HHG spectra. The blue circles in Fig. 5(b), representing the actual pulse $\Delta T$ values, show excellent agreement with the predictions of our model (red diamond line). This strong correspondence not only confirms the validity of our model but also suggests a practical approach for experimentally generating non-integer HHG.

It should be noted that the deviation between the calculated and real $\Delta T$ values increases with pulse width. This discrepancy primarily stems from two factors: the non-uniform intensity distribution of HHG sidebands and the distortion of sideband spacing caused by degraded spectral resolution. These effects become especially significant for long pulses, thereby limiting the accuracy of $\Delta T$ extraction in this regime.

### 3.3. Optical frequency comb case

The optical frequency comb technique provides an alternative approach for generating non-integer HHG. Within our multi-MSFD-like framework, these phenomena can be fundamentally explained. In this scheme, a laser emits phase-coherent, equally spaced frequency components (the "comb"). When interacting with a target medium (e.g., gas atoms), this periodic structure induces harmonic emission at non-integer multiples of the fundamental frequency. The phase coherence of the frequency comb ensures constructive interference at specific frequencies, thereby generating well-defined sidebands around the primary harmonics. This mechanism enables precise spectral control in HHG, with the sideband spacing governed by the comb repetition frequency.

The total HHG signal generated by the interaction between the target and an optical frequency comb pulse consisting of $K$ separated IR pulses can be expressed as

$$H(\omega) = H_0 + H_1 e^{i\omega\Delta t_5} + H_2 e^{i2\omega\Delta t_5} + \cdots + H_{K-1} e^{i(K-1)\omega\Delta t_5}, \tag{9}$$

where $\Delta t_5$ represents the time delay between two adjacent IR pulses. Each term corresponds to the resultant amplitude from a single IR pulse, representing a single-MSFD-like HHG emission. Assuming equal amplitudes for all emission clusters (i.e., $H_0 = H_1 = H_2 = \cdots = H_{K-1} = c$), the total HHG signal simplifies to

$$H(\omega) = c \sum_{S=1}^{K} e^{i(S-1)\omega\Delta t_5}. \tag{10}$$

By substituting $\omega\Delta t_5 = \frac{\omega}{\omega_0}\omega_0\Delta t_5 = 2\pi N\Delta T$, where $N$ is the HHG order, we obtain

$$H(\omega) = c \sum_{S=1}^{K} e^{i2\pi(S-1)N\Delta T}. \tag{11}$$

Consistent with our previous analysis, the relationship between $\Delta N$ and $\Delta T$ remains

$$\Delta N = \frac{1}{\Delta T}. \tag{12}$$

This result demonstrates that for HHG generated by an optical frequency comb laser, the sideband spacing $\Delta N$ in the HHG spectrum is inversely proportional to the time delay between neighboring IR pulses.

A careful re-examination of Eq. (11) reveals that the constructive interference condition occurs when each phase factor $e^{i(S-1)N\Delta T}$ in the summation $\sum_{S=1}^{K} e^{i(S-1)N\Delta T}$ equals unity. The progressive increase of the index $(S-1)$ from 0 to $K-1$ introduces strong sensitivity to small deviations: for given $N$ and $\Delta T$ satisfying constructive interference, even a small deviation $dN$ becomes magnified as $(S-1)dN\Delta T$ grows with

increasing $S$. This effect is particularly pronounced for large $S$, where the accumulated phase shift causes the exponential term to deviate substantially from unity. As the number of contributing pulses ($K$) increases, the summation exhibits enhanced sensitivity to small deviations, leading to rapid amplitude decay away from the exact constructive interference conditions. Consequently, systems with larger numbers of pulses exhibit sharper roll-off of harmonic intensity near maxima, more pronounced peak narrowing in the HHG spectrum, and enhanced spectral resolution in the optical frequency comb.

Numerical simulation results are shown in Fig. 6. Figure 6(a) illustrates three optical frequency comb pulse configurations consisting of 2, 4, and 8 Gaussian sub-pulses, respectively. Each sub-pulse features a peak intensity of 0.092 a.u., a central wavelength of 800 nm, and a pulse duration of 2 o.c. (FWHM). The sub-pulses are equally spaced with a fixed temporal separation of 8 o.c. (denoted as $\Delta T = 8$ o.c. in our theoretical model).

As shown in Fig. 6(b), the HHG spectra produced by these pulse sequences exhibit well-defined optical frequency comb structures with a characteristic sideband spacing of $\Delta N = 0.125$. This value shows exact agreement with the theoretical prediction from Eq. (12). Notably, the value of $\Delta N$ remains constant across all pulse configurations, independent of the total number of sub-pulses, further validating the universality of Eq. (12).

Furthermore, the spectral linewidth of the comb teeth progressively narrows as the number of sub-pulses increases. Physically, this linewidth reduction corresponds to the increasing number of harmonic emission clusters ($S$) participating in the generation process. The observed spectral sharpening effect quantitatively matches the behavior predicted by our analysis of Eq. (11).

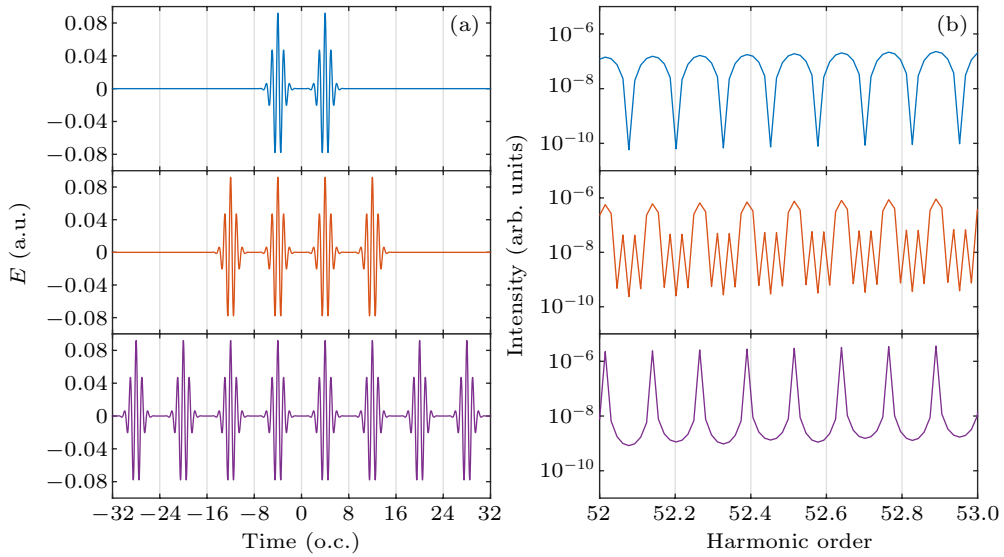



**Fig. 6.** (a) Laser pulse sequences with varying numbers of sub-pulses (2, 4, and 8) while maintaining identical inter-pulse spacing and laser parameters. The temporal separation between adjacent sub-pulses is fixed at 8 o.c. (b) HHG spectra produced by the laser fields shown in panel (a). The spectra reveal distinct frequency comb structures whose spectral linewidth progressively narrows with increasing number of sub-pulses, while maintaining constant peak positions and uniform spacing. The characteristic sideband separation corresponds to a harmonic-order interval of $\Delta N = 0.125$ between adjacent comb peaks.

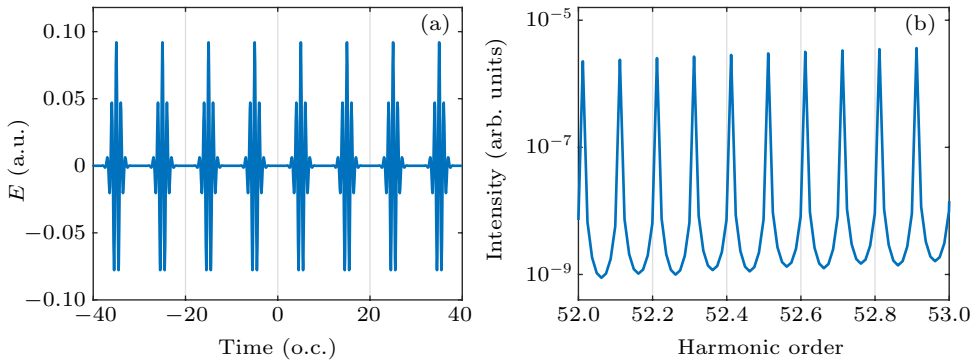



**Fig. 7.** (a) The pulse spacing of the 8-pulse train in Fig. 6(a) was adjusted to 10 o.c. while maintaining all other laser parameters unchanged. (b) HHG spectrum produced by the laser pulse shown in panel (a). The frequency comb exhibits a peak separation of 0.1 in harmonic order, which exactly equals 1/10.

As shown in Fig. 7(a), we employ an optical frequency comb pulse consisting of eight sub-pulses with a temporal separation of $\Delta T = 10$ o.c. The laser parameters of each sub-pulse are identical to those in Fig. 6(a). The corresponding HHG spectrum is displayed in Fig. 7(b), exhibiting a harmonic order spacing of $\Delta N = 0.1$. This value precisely matches $1/10$, in full agreement with the theoretical prediction of Eq. (12). These results demonstrate that our model not only accurately predicts the peak spacing in the HHG spectrum but also provides a coherent explanation for the observed variations in spectral bandwidth.

## 4. Conclusion

In summary, we propose a novel optical temporal interference model (OTIM) for understanding and controlling non-integer high-harmonic generation (HHG). By drawing an analogy with the multi-slit Fraunhofer diffraction (MSFD) principle, this model unifies the physical mechanisms underlying three distinct non-integer HHG generation schemes: the single-pulse scheme corresponds to a single-slit-like MSFD process, the pulse-shaping scheme to a double-slit-like MSFD process, and the optical frequency comb scheme to a multi-slit-like MSFD process. The model not only successfully predicts the emergence of sidebands in HHG spectra but also establishes a quantitative relationship between the temporal characteristics of driving laser pulses and the resulting non-integer HHG spectra, providing a powerful tool for precise control of non-integer HHG.

Compared to existing models, the OTIM possesses distinct advantages: rooted in classical geometric optics principles, it provides a more intuitive and physically clear interpretation of HHG spectral features. This capability significantly enhances our understanding of non-integer HHG mechanisms. Notably, the model can explain the bandwidth characteristics of optical frequency combs and precisely calculate the comb-tooth spacing. Unlike conventional methods that employ long pulse trains to generate frequency combs, our approach achieves similar comb structures using a single $\pi$-phase-modulated Gaussian pulse. Using this model, we can accurately design shaped pulses to generate optical frequency combs with specific tooth spacing, offering a novel approach to producing custom optical comb structures.

## Acknowledgments

This project was supported by the National Natural Science Foundation of China (Grant No. 12304379), the Natural Science Foundation of Liaoning Province (Grant No. 2024-BS-269), and the Guangdong Basic and Applied Basic Research Foundation (Grant No. 025A1515011117).

## References

[1] Udem T, Holzwarth R and Hänsch T 2002 *Nature* **416** 233
[2] Margolis H S 2009 *J. Phys. B* **42** 154017
[3] Yao Y, Li B, Yang G, Chen X, Hao Y, Yu H, Jiang Y and Ma L 2021 *Photon. Res.* **9** 98
[4] Pupeza I, Zhang C, Högner M and Ye J 2021 *Nat. Photonics* **15** 175
[5] Chang L, Liu S and Bowers J E 2022 *Nat. Photonics* **16** 95
[6] Shao X D, Yan Y, Han H and Wei Z 2024 *Astron. Tech. instrum.* **1** 105
[7] Spencer D T, Drake T, Briles T C, *et al.* 2018 *Nature* **557** 81
[8] Cai Y, Roslund J, Thiel V, Fabre C and Treps N 2021 *npj Quantum Inf.* **7** 82
[9] Kang G, Lee Y, Kim J, Yang D, Nam H K, Kim S, Baek S, Yoon H, Lee J, Kim T T and Kim Y J 2024 *Nanophotonics* **13** 983
[10] Hiraoka T, Inose Y, Arikawa T, Ito H and Tanaka K 2022 *Nat. Commun.* **13** 3740
[11] Yun C, Teng H, Zhang W, Zhan M, Han H, Zhong X, Wei Z, Wang B and Hou X 2010 *Chin. Phys. B* **19** 124210
[12] Bertrand J, Wörner H J, Bandulet H C, Bisson E, Spanner M, Kieffer J C, Villeneuve D and Corkum P B 2011 *Phys. Rev. Lett.* **106** 023001
[13] Ghimire S, DiChiara A D, Sistrunk E, Agostini P, DiMauro L F and Reis D A 2011 *Nat. Phys.* **7** 138
[14] Tudorovskaya M and Lein M 2017 *Phys. Rev. A* **95** 043418
[15] Qiao Y, Wang J, Yan Y, Song S, Chen Z, Liu A, Chen J, Guo F and Yang Y 2022 *Chin. Phys. B* **31** 064214
[16] Wang S, Guo J, He X, Liang Y, Xie B, Zhong S, Teng H and Wei Z 2023 *Chin. Phys. B* **32** 063301
[17] Huang P C, Hernández-García C, Huang J T, Huang P Y, Lu C H, Rego L, Hickstein D D, Ellis J L, Jaron-Becker A, Becker A, Yang S D, Durfee C G, Plaja L, Kapteyn H C, Murnane M M, Kung A H and Chen M C 2018 *Nat. Photon.* **12** 349
[18] Ren Z, Zhang B, Yang Y, Zhu Y, Zhao J and Zhao Z 2023 *Results Phys.* **55** 107181
[19] Torres R, Kajumba N, Underwood J G, Robinson J S, Baker S, Tisch J W G, de Nalda R, Bryan W A, Velotta R, Altucci C, Turcu I C E and Marangos J P 2007 *Phys. Rev. Lett.* **98** 203007
[20] Zhang R, Wang F, Yuan H, Chen S, Yang C, Ou T, Song J, Liao Q and Lu P 2024 *Phys. Rev. A* **109** 043118
[21] Liang C T, Zhang J J and Li P C 2023 *Chin. Phys. B* **32** 033201
[22] Wörner H J, Bertrand J B, Kartashov D V, Corkum P B and Villeneuve D M 2010 *Nature* **466** 604
[23] Le A T, Morishita T, Lucchese R and Lin C D 2012 *Phys. Rev. Lett.* **109** 203004
[24] Wagner N L, Wüest A, Christov I P, Popmintchev T, Zhou X, Murnane M M and Kapteyn H C 2006 *Proc. Natl. Acad. Sci.* **103** 13279
[25] Phan N L, Le C T, Hoang V H and Le V H 2019 *Phys. Chem. Chem. Phys.* **21** 24177
[26] Qiao Y, Chen J, Zhou S, Chen J, Jiang S and Yang Y 2024 *Chin. Phys. Lett.* **41** 014205
[27] Takahashi E J, Kanai T, Ishikawa K L, Nabekawa Y and Midorikawa K 2007 *Phys. Rev. Lett.* **99** 053904
[28] Kfir O, Grychtol P, Turgut E, Knut R, Zusin D, Popmintchev D, Popmintchev T, Nembach H, Shaw J M, Fleischer A, Kapteyn H, Murnane M and Cohen O 2015 *Nat. Photon.* **9** 99
[29] Ge X L, Du H, Wang Q, Guo J and Liu X S 2015 *Chin. Phys. B* **24** 023201
[30] Zhong H Y, Guo J, Zhang H D, Du H and Liu X S 2015 *Chin. Phys. B* **24** 073202
[31] Zhao X, Wang S J, Yu W W, Wei H, Wei C, Wang B, Chen J and Lin C D 2020 *Phys. Rev. Appl.* **13** 034043
[32] Zhao X, Li S, Driver T, Hoang V H, Le A T, Cryan J P, Marinelli A and Lin C D 2022 *Phys. Rev. A* **105** 013111
[33] Fu W, Yu J, Li R, Li B, Lai Y H and Li W 2024 *ACS Photonics* **11** 53
[34] Ghimire S and Reis D A 2019 *Nat. Phys.* **15** 10
[35] Weissenbilder R, Carlström S, Rego L, *et al.* 2022 *Nat. Rev. Phys.* **4** 713
[36] Wang L, Wang X W, Xiao F, Wang J C, Tao W K, Zhang D W and Zhao Z X 2023 *Chin. Phys. Lett.* **40** 113201
[37] Chen J Q, Jiang W L, Qiao Y, Yang Y J and Chen J G 2025 *Chin. Phys. Lett.* **42** 013201
[38] Zhang C P and Miao X Y 2023 *Chin. Phys. Lett.* **40** 124201
[39] Borrego-Varillas R, Lucchini M and Nisoli M 2022 *Rep. Prog. Phys.* **85** 066401
[40] Wang L, Xiao F, Song P, Tao W K, Sun X, Wang J C, Zheng Z G, Zhao J, Wang X W and Zhao Z X 2023 *Chin. Phys. Lett.* **40** 114203

[41] Zhao J, Liu J L, Wang X W, Yuan J M and Zhao Z X 2022 *Chin. Phys. Lett.* **39** 123201

[42] Fu T T, Zhou S S, Chen J G, Wang J, Guo F M and Yang Y J 2023 *Opt. Express* **31** 30171

[43] Klemke N, Tancogne-Dejean N, Rossi G M, *et al.* 2019 *Nat. Commun.* **10** 1319

[44] Hu H, Li N, Liu P, Li R and Xu Z 2017 *Phys. Rev. Lett.* **119** 173201

[45] Yang Y, Lu J, Manjavacas A, Luk T S, Liu H, Kelley K, Maria J P, Runnerstrom E L, Sinclair M B, Ghimire S and Brener I 2019 *Nat. Phys.* **15** 1022

[46] Qiao Y, Chen J, Li Z, *et al.* 2024 *Opt. Lett.* **49** 3986

[47] Nourbakhsh Z, Tancogne-Dejean N, Merdji H and Rubio A 2021 *Phys. Rev. Appl.* **15** 014013

[48] Calegari F, Sansone G, Stagira S, Vozzi C and Nisoli M 2016 *J. Phys. B* **49** 062001

[49] Maiuri M, Garavelli M and Cerullo G 2019 *J. Am. Chem. Soc.* **142** 3

[50] Chini M, Zhao K and Chang Z 2014 *Nat. Photon.* **8** 178

[51] Paul P M, Toma E S, Breger P, *et al.* 2001 *Science* **292** 1689

[52] Feng X, Gilbertson S, Mashiko H, *et al.* 2009 *Phys. Rev. Lett.* **103** 183901

[53] Han J, Tang X, Yin Z, Wang K, Fu Y, Wang B, Chen Y, Zhang C and Jin C 2022 *Opt. Express* **30** 47942

[54] Silva R, Blinov I V, Rubtsov A N, Smirnova O and Ivanov M 2018 *Nat. Photon.* **12** 266

[55] Xing M, Wang J, Zhao X and Zhou S S 2025 *Chin. Phys. Lett.* **42** 043201

[56] Raith P, Ott C, Anderson C P, Kaldun A, Meyer K, Laux M, Zhang Y, Pfeifer T 2012 *Appl. Phys. Lett.* **100** 121104

[57] Schmid C P, Weigl L, Grössing P, *et al.* 2021 *Nature* **593** 385

[58] Xia C L, Lan Y Y and Miao X Y 2021 *Chin. Phys. B* **30** 043202

[59] Lange C S, Hansen T and Madsen L B 2024 *Phys. Rev. A* **109** 063103

[60] Carrera J J, Son S K and Chu S I 2008 *Phys. Rev. A* **77** 031401

[61] Carrera J J and Chu S I 2009 *Phys. Rev. A* **79** 063410

[62] Chiril C C, Dreissigacker I, van der Zwan E V and Lein M 2010 *Phys. Rev. A* **81** 033412

[63] Born M and Wolf E 2019 *Principles of Optics* (Cambridge: Cambridge Univ. Press)

[64] Lewenstein M, Balcou P, Ivanov M Y, L'Huillier A and Corkum P B 1994 *Phys. Rev. A* **49** 2117

[65] Li Q, Li Y, Guo F, *et al.* 2024 *Phys. Rev. A* **109** 063112

[66] Weiner A M 2000 *Rev. Sci. Instrum.* **71** 1929